Physics Letters A 490 (2023) 129193

Contents lists available at ScienceDirect

Physics Letters A

journal homepage: www.elsevier.com/locate/pla

Hopping tunneling through a quasiperiodic potential

M. Cruz-Méndez [a], H. Cruz [b,*]

[a] Escuela Politécnica Superior, Universidad Francisco de Vitoria, Ctra. Pozuelo-Majadahonda Km. 1.800, 28223 Pozuelo de Alarcón, Madrid, Spain
[b] Departamento de Física, IUDEA, Universidad de La Laguna, Avda. Astrofísico Francisco Sánchez s/n, 38204 La Laguna, Tenerife, Spain

ARTICLE INFO

Communicated by L. Ghivelder

Keywords:
Localization effects
Tunneling
Quasiperiodic systems

ABSTRACT

In this work, we have developed a one-dimensional tight-binding model to investigate the conductivity of tunneling through a quasiperiodic or slowly-varying potential. Our study focuses on the hopping tunneling properties of a tight-binding model in which the on-site potential is replaced by both quasiperiodic and periodic functions. By comparing the hopping transport in scenarios involving a periodic potential and an slowly-varying model, the latter being the only known case of a 1D potential with a mobility edge and a metal-insulator transition, we gain valuable insights. In our analysis, we consider a proposed device situated between two quantum reservoirs in both quasiperiodic and periodic cases. Remarkably, we find that the tunnel transport through the lattice completely diminishes at the band center. This intriguing phenomenon is likely to hold fundamental importance in the interpretation of experimental data.

1. Introduction

Since the seminal work of Anderson [1], the investigation of quantum localization has remained a central paradigm in Condensed Matter Physics. Despite extensive studies of the localization phenomenon, many open questions persist in this research field. Two fundamental models, the Anderson model and the Aubry-André incommensurate potential, deserve mention. In the Anderson model, disorder manifests as random amplitudes in the on-site positions of a lattice. Conversely, in the Aubry-André model [2], disorder arises from a potential function that is incommensurate with the underlying lattice. Localization effects in this scheme can be attributed to both the destructive interference associated with multiple scattering processes of a particle traveling through an incommensurate medium and the spectral properties of its Schrödinger equation [3]. In recent times, this subject has garnered significant attention, primarily fueled by the prospects of pioneering experimental research employing optical lattices and cold atom gases [4–7]. An intimately related and intriguing localization problem is presented by the Aubry-André model in optical lattices, which exhibits a metal-insulator transition when the strength of the periodic potential is varied [8–11]. Utilizing ultracold bosons [12,13], researchers have delved into the study of delocalization effects in the Aubry-André model.

Optical lattices, constructed from light, serve as crystalline structures capable of trapping atoms at extremely low temperatures [14]. Unlike conventional solid-state crystals, an optical lattice arises from the interference of laser beams, boasting dimensions approximately 1,000 times larger. Within this lattice, trapped atoms emulate the behavior of electrons within a solid, exhibiting the ability to tunnel through potential barriers formed by the laser beams.

The potential of an optical lattice emerges through the coherent interaction of two laser beams propagating in opposing directions. Depending on the light frequency, ultracold atoms can be confined to specific spatial regions. One of the most valuable applications of optical lattices lies in their capacity to realize simplified models of Condensed Matter Physics within experimental settings. Ultracold gas experiments benefit greatly from optical lattices as they permit easy control of crucial factors like interatomic interaction and band structure by manipulating external laser beams [15–18].

In addition to optical lattices, solid-state superlattices have garnered significant attention in recent years due to their potential applications as novel optical and electrical devices [19–23]. A solid-state superlattice structure involves the growth of two different materials in alternating layers, where the lattice constant of both materials must closely match to achieve a crystalline structure. One layer of the material acts as a potential barrier, while the other functions as a quantum well within the structure. The coupling between these quantum wells can give rise to an artificial conduction miniband. Recent studies have inferred the existence of phonon Anderson localization in Si/Ge aperiodic superlattices through overall thermal conductivity behaviors [24–26]. Hu et al. [25]

* Corresponding author.
E-mail address: hcruz@ull.edu.es (H. Cruz).

https://doi.org/10.1016/j.physleta.2023.129193
Received 4 September 2023; Received in revised form 10 October 2023; Accepted 22 October 2023
Available online 24 October 2023

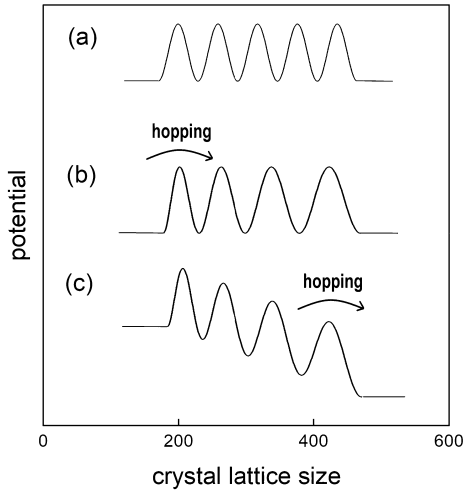

Fig. 1. An illustration of a one-dimensional periodic and quasiperiodic potential placed between two reservoirs. (a) Periodic case. (b) Slowly-varying potential or aperiodic case. For an optical lattice, the end sites are driven by ultracold atomic reservoirs. The quasiperiodic potential shows a slow variation with the number of lattice sites. (c) Quasiperiodic potential in a solid-state superlattice case. An external electric field is applied between the contacts.

observed a decreasing trend in the overall thermal conductivity with respect to device length, indicating the potential presence of phonon Anderson localization in solid-state superlattices.

However, observing Anderson and Aubry-André localizations in real materials, particularly superlattices, presents challenges due to the suppression of disorder effects caused by various quantum phenomena [4]. Furthermore, creating superlattice potentials with a slowly-varying superlattice period proves to be highly challenging. The growth of materials with such a slowly-varying superlattice period to realize functional devices within a laboratory setting is a formidable task [27,28]. As a result, investigating alternative approaches to study localization phenomena becomes essential, allowing us to gain insights into these intriguing phenomena in a more controllable and experimentally accessible manner.

In the experimental setup, an optical lattice is incorporated between two cold-atom reservoirs to investigate the conductivity of ultracold atoms through a quasiperiodic potential (Fig. 1). By imposing a chemical potential difference between the end sites, atomic transport is induced throughout the system [29]. Similarly, in the superlattice scenario, a layered material is positioned between two electronic contacts, and an external electric field is applied between the electrodes (Fig. 1). In both cases involving ultracold atoms and electrons, the quasiperiodic potential is inserted between two atomic or electronic reservoirs, respectively.

In order to accurately characterize the current flow within such devices, it is imperative to incorporate quantum transport phenomena between the contacts and the lattice. Initially, electrons or cold atoms from the reservoir can tunnel through the lattice potential barriers as a first approximation (Fig. 1). The tunneling amplitude is directly related to the degree of wave function overlap between the reservoir and the quasiperiodic wave functions. In this context, we can adopt a hopping-tunneling model to effectively describe the injection of electric charge (or cold atoms) at a device contact.

Until now, the existence of a metal-insulator transition in experimental studies remains elusive. Moreover, an unsolved and crucial challenge in the research area revolves around assessing the hopping tunneling between an aperiodic potential and the electron or cold-atom reservoirs. The role of transport tunneling in these experiments cannot be underestimated. In this work, we aim to evaluate the conductivity of cold atoms or electrons through a slowly-varying potential by determining the average extension of eigenstates near the lattice borders. We will compare our results with Lyapunov exponent calculations. Through this analysis, we will demonstrate that hopping tunneling plays a pivotal role in comprehending experiments involving quasiperiodic potentials. By shedding light on these aspects, we strive to contribute valuable insights into the fundamental mechanisms underlying the behavior of quantum particles in the presence of quasiperiodic potentials.

2. Model

In this work, the physical systems under study are represented by the following Hamiltonian:

$$H = \sum_{i=1}^{N-1} t\left(|i><i+1| + |i-1><i| \right) + V_i\, |i><i| \,, \tag{1}$$

Here, H describes a single-particle moving on a one-dimensional lattice with a t matrix element connecting each lattice site to its two nearest neighbors. The term V_i in Eq. (1) introduces a modulation of the on-site energies with amplitude V_i.

Essentially, Eq. (1) corresponds to the tight-binding model applied to a chain of ultracold atoms or quantum wells in a solid-state superlattice (see Fig. 1). The tight-binding equation is given by:

$$t\,(u_{n-1} + u_{n+1}) + V_n u_n = E u_n \,, \tag{2}$$

where u_n represents the amplitude of the carrier wave function at the n-th lattice site, and V_n is the on-site potential. In this work, we consider two different models.

The first on-site potential, denoted as V_n, is an Aubry-André model. We shall consider a variation of the original Aubry-André potential proposed by Das Sarma et al. [27]. The original Aubry-André model presents only a metal-insulator transition. The model proposed by Das Sarma et al. [27] exhibits a mobility edge and a metal-insulator transition with a gapless Schrödinger spectrum.

The most important characteristic of this potential is that it exhibits a metal-insulator transition for $\lambda < 2$ and $\nu < 1$. The mobility edges are located at energies $E_c = \pm|2 - \lambda|$. Eigenstates at the band center, $|E| < |E_c|$, are all extended, whereas the band-edge states ($|E| > |E_c|$) are all localized. Such a slowly-varying potential exhibits neither periodic nor random characteristics and can be expressed as follows:

$$V_n = \lambda \cos(\pi \alpha n^{\nu}) \tag{3}$$

where α is a real number, λ represents the strength of the potential ($0 \leq \lambda \leq 2$), and ν is a parameter ranging between 0 and 1. As depicted in Fig. 1, the potential varies with the number of lattice sites. If $\nu = 1$ in Eq. (3), we have an almost periodic potential.

We should point out that $\pi\alpha$ has been taken to be equal to a real number in this work. Taking into account that n is an integer and N a finite number, when $\nu = 1$, the potential is (almost) periodic. Strictly speaking, it is not periodic. Conversely, when $\nu < 1$, the potential will be referred to in the manuscript as slowly-varying, quasiperiodic, aperiodic, or Aubry-André type.

Remarkably, such a slowly-varying model represents the sole instance of a one-dimensional tight-binding potential featuring a metal-insulator transition with mobility edges located at $E_c = \pm|2 - \lambda|$, where λ is the potential perturbation.

The original Aubry-André potential is $V_n = \lambda \cos(\pi \alpha' n)$, where α' is an irrational number ($\alpha' = 1 + \sqrt{5}$) and λ represents the strength of the potential. When α' is an irrational number, Bloch's theorem is no longer applicable, and the calculation of the spectrum is not trivial. The eigenvalue spectrum is fractal, and the famous Hofstadter butterfly is obtained [27].

A related quantity, the normalized density of states, denoted by $\rho(E)$, can now be introduced:

$$\rho(E) = \frac{1}{N} \sum_{j=1}^{N} \delta(E - E_j) \,, \tag{4}$$

where N is the number of sites. The density is normalized to 1. To calculate the density of states, we approximate $\delta(E-E_j)$ with a normalized Gaussian function [30–32]:

$$\delta(E-E_j)=\frac{1}{\sigma\sqrt{2\pi}}\exp\left[-\frac{(E-E_j)^2}{2\sigma^2}\right]. \tag{5}$$

In this work, σ is taken to be equal to $\sigma=0.015$. Here, E_j represents the obtained eigenvalues with $j\in 1,2,...,N$.

In real materials, the Lyapunov exponent $\gamma(E)$ has been widely used to characterize extended and localized quantum states. The Lyapunov exponent is defined as the inverse of the localization length [30–32], providing insights into the asymptotic behavior of the eigenstates:

$$\gamma(E_j)=\frac{1}{N-1}\sum_{j\neq l} ln\,|E_j-E_l|, \tag{6}$$

where N represents the number of sites in the lattice. For extended states and below a mobility edge, $\gamma(E_j)=0$. In contrast, in a localized state with energy E_j, $\gamma(E_j)$ possesses a finite value.

Solving Eq. (2) provides different eigenvectors $u_n(E_j)$ corresponding to each distinct eigenvalue E_j, where $j\in 1,2,...,N$ and $n\in 1,2,...,N$. The obtained eigenvectors are normalized, i.e.,

$$\sum_{n=1}^{N}|u_n(E_j)|^2=1\,. \tag{7}$$

In our model, the obtained eigenvalues are ordered in energy (from minimum to maximum energy). Specifically, $j=1$ corresponds to E_1, which represents the eigenvalue with the minimum energy, and E_N corresponds to the maximum energy eigenvalue, with $j=N$.

It is noteworthy that a unique property of the Aubry-André model is its manifestation of a metal-insulator transition. One method to demonstrate this is by calculating the inverse participation ratio (IPR) of all eigenstates. This quantity is specifically designed to characterize the localization properties of a cold-atom eigenstate. The IPR vanishes for spatially extended states while remaining finite for localized states [33]. Additionally, a quantity denoted as σ_c, accounting for the average extension of eigenstates in bichromatic optical lattices, has been utilized by Boers et al. [34].

These quantities and indices mentioned above provide an evaluation of the wave function extension across all sites of an Aubry-André model. They account for the amplitude u_n of the wave function at each lattice site for every eigenstate. However, we acknowledge that the u_n values near the reservoirs may significantly influence the hopping tunneling process.

With this consideration, we introduce the number of states $\mathcal{N}$ at each i-lattice site within a range of energies:

$$\mathcal{N}_n(m_i,m_f)=\sum_{j=m_i}^{m_f}|u_n(E_j)|^2 \tag{8}$$

in this work. Here, j ranges from m_i to m_f, with the maximum value for $\mathcal{N}_n$ at an n-lattice site being N, where $j\in 1,2,...,N$. Within a defined energy interval (m_i,m_f), $\mathcal{N}_n$ represents the sum of probabilities of finding an electron or ultracold atom at an n-lattice position. In other words, $\mathcal{N}_n$ is proportional to the carrier probability densities $|u_n|^2$ within the specified energy range.

The eigenvalues are ordered in energy. Every 25 consecutive states are grouped to calculate a $\mathcal{N}_{50}$ value. The energy associated with such a $\mathcal{N}_{50}$ quantity is the eigenenergy of the first element of the list. For example, E_1 is the energy associated with the $E_1,...,E_{25}$ group and so on. This way, the energy of each 25 consecutive eigenvalues is approximated by a unique value. The approach has been tested considering groups of 50 and 100 elements as well. We achieved convergence for 25 eigenvalues with an error of less than 5%. In Figs. 9 and 10, we have plotted 20 points for the $\mathcal{N}_{50}$ value and $\gamma(E)$ for $-2<E<2$.

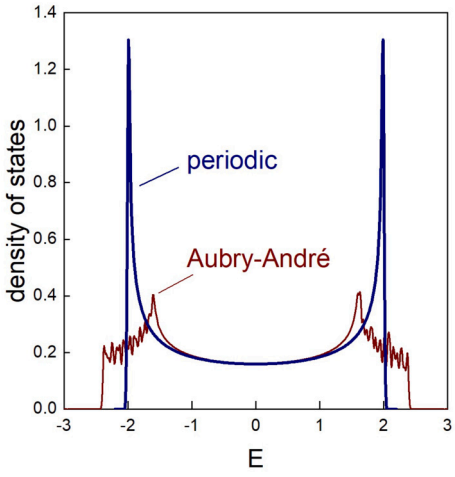

Fig. 2. Density of states versus energy for a periodic potential ($\lambda=0$) and for an Aubry-André potential ($\lambda=0.4$). We have taken $\pi\alpha=0.4$ and $\nu=0.7$ for the slowly-varying potential in Eq. (3). The mobility edge is at $E=\pm1.6$ in the quasiperiodic case. In the periodic case, λ is set to $\lambda=0$.

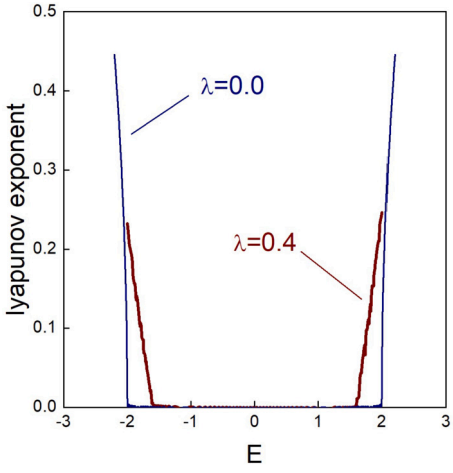

Fig. 3. Lyapunov exponent versus energy for a periodic potential ($\lambda=0$) and for an Aubry-André model ($\lambda=0.4$). In the aperiodic case, we have taken $\pi\alpha=0.4$ and $\nu=0.7$. The metal-insulator transition occurs at $E=\pm1.6$ in the slowly-varying case.

3. Results

The Hamiltonian described in Eq. (1) is solved to obtain the eigenenergies and eigenvalues. Fig. 2 illustrates the density of states versus energy for an slowly-varying model ($\lambda=0.4$) and a periodic potential ($\lambda=0$). In the quasiperiodic case, we set $\nu=0.7$ and $\lambda=0.4$. The figure clearly exhibits the existence of mobility edges in the system, where the singular points of the density of states are located at $E_c=\pm1.6$. Additionally, Fig. 3 shows the Lyapunov exponent versus energy, demonstrating that the mobility edges are also situated at $E_c=\pm1.6$ in the quasiperiodic case ($\nu=0.7$). When the energy passes through the mobility edges, a dramatic change is observed.

For a free-particle model ($\lambda=0$), the maximum and minimum eigenvalues are $2t$ and $-2t$, respectively. However, Fig. 2 illustrates a finite value for the density of states for $|E|>2t$. We observe two tails in the density of states at $E=\pm2t$. This numerical effect can be explained by considering that Eqs. (4) and (5) were used to construct our density of states. It should be noted that a normalized Gaussian function was employed for each eigenvalue. Consequently, states near the $\pm2t$ band limit contribute to the tails of the density of states. Fig. 2 also presents

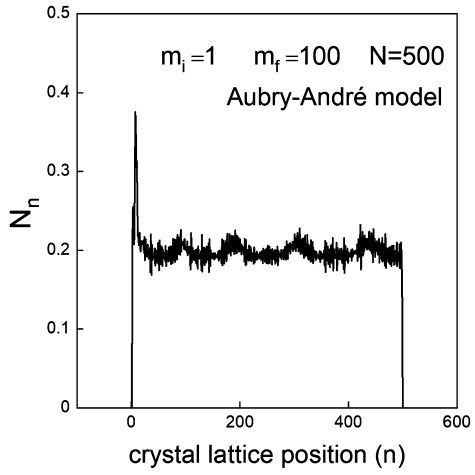

Fig. 4. $\mathcal{N}_n(m_i, m_f)$ versus crystal lattice position (n). The m_i and m_f values have been taken to be equal to 1 and 100, respectively. In the Aubry-André model: $\pi\alpha = 0.4$, $\lambda = 0.4$ and $\nu = 0.7$.

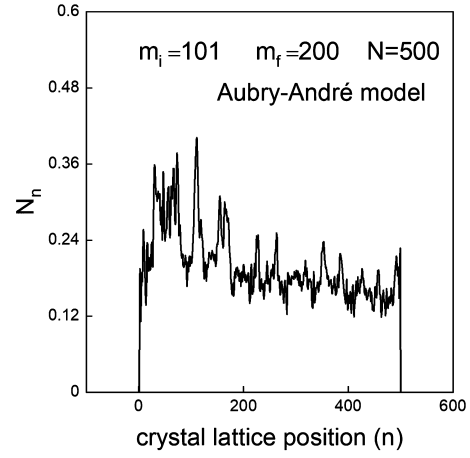

Fig. 5. $\mathcal{N}_n(m_i, m_f)$ versus crystal lattice position (n). The m_i and m_f values have been taken to be equal to 101 and 200, respectively. In the Aubry-André model: $\pi\alpha = 0.4$, $\lambda = 0.4$ and $\nu = 0.7$.

a slowly-varying potential with $\lambda = 0.4$. In this case, it is clearly shown that the absolute band edges are located at $E = \pm(2 + |\lambda|)$.

Fig. 3 also displays Lyapunov exponent values greater than zero for a periodic potential ($\lambda = 0$) where all states are extended. This phenomenon arises because $\gamma(E)$ has been evaluated in places where eigenvalues do not exist, such as at $|E| > 2t$ in the periodic case. This occurs because it is possible to replace E_j with an arbitrary E value in Eq. (3). This representation provides a better portrayal of the Lyapunov exponent, as depicted in Figs. 2 and 3.

Our slowly-varying model exhibits extended states near the band center ($-E_c < E < E_c$) and localized states at the band edges ($|E| > E_c$), with mobility edges located at $\pm E_c = \pm(2 - |\lambda|)$. The absolute band edges are at $\pm(2 + |\lambda|)$, with the origin of energies taken to be at the band center. The slowly varying nature of the potential, defined by Equation (3), contributes to the localization or extension of eigenstates due to its aperiodic characteristics [30–32].

Fig. 4 presents $\mathcal{N}_n$ versus the crystal lattice site (n). For the calculation, we considered the first 100 eigenvectors and eigenvalues ($m_i = 1$ to $m_f = 100$ in Eq. (8)). The plot demonstrates that $\mathcal{N}_n$ has a finite value within an energy range at each crystal site. A similar result is obtained in the subsequent energy interval ($m_i = 101, m_f = 200$) (Fig. 5). In both cases (Fig. 4 and 5), $\mathcal{N}_n$ does not vanish along the lattice.

However, Fig. 6 shows a distinct outcome. It displays the number of states versus n in the band center for the energy range (201, 300).

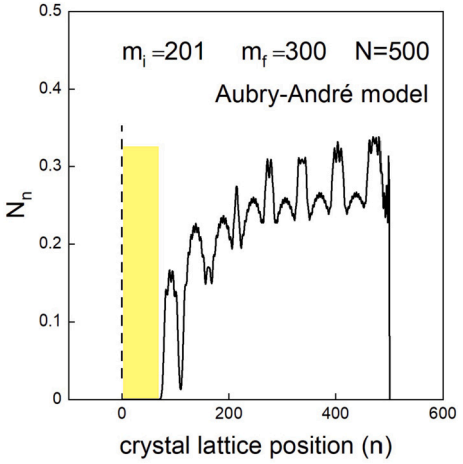

Fig. 6. $\mathcal{N}_n(m_i, m_f)$ versus crystal lattice position (n). The m_i and m_f values have been set to 201 and 300, respectively. In the Aubry-André model: $\pi\alpha = 0.4$, $\lambda = 0.4$, and $\nu = 0.7$. The dashed line represents the left border of the optical lattice. The yellow stripe indicates the lattice sites in which the carrier probability density vanishes.

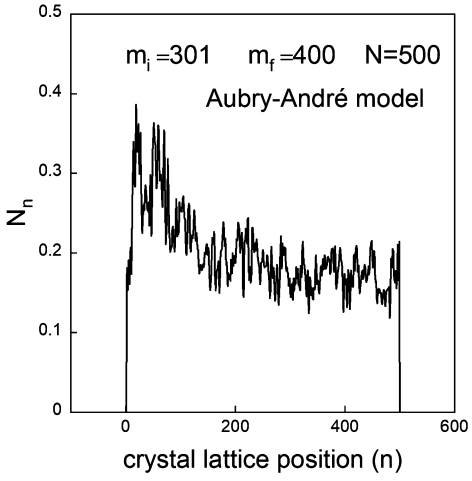

Fig. 7. $\mathcal{N}_n(m_i, m_f)$ versus crystal lattice position (n). The m_i and m_f values have been set to 301 and 400, respectively. In the Aubry-André model: $\pi\alpha = 0.4$, $\lambda = 0.4$, and $\nu = 0.7$.

Notably, $\mathcal{N}_n$ vanishes in the lattice sites located near the left end site, as indicated by a dashed line in Fig. 6. Consequently, hopping tunneling between the left reservoir and the crystal potential can be neglected. Tunneling transport is proportional to the wave function overlapping between reservoir eigenstates and $|u_n|^2$, i.e., is proportional to $\mathcal{N}_n$.

For the energy intervals (301, 400) and (401, 500), the probability density $\mathcal{N}_n$ has non-null values at different lattice site positions (Figs. 7 and 8). This phenomenon can be attributed to the asymmetry of the potential described by Eq. (3). Figs. 3-8 provide new insights for the slowly-varying model, as it is the only known case of a 1D potential with a metal-insulator transition and a mobility edge. The carrier probability density in the lattice sites near the left contact increases with an increase in $|E|$. Conversely, $\mathcal{N}_n$ in the lattice positions near the left end site decreases as $|E|$ is decreased. The origin of energies is taken to be at the band center. It is important to note that the left end site corresponds to the highest value for the potential frequency (see Fig. 1). The potential is asymmetric, with $\nu < 1$ in Eq. (3).

In Figs. 3-8, it is evident that hopping transport from the left reservoir (Fig. 1) is forbidden at the band center, around $E = 0$. Surprisingly, the Lyapunov exponent indicates that the eigenvectors are extended states at the band center (Fig. 3). This discrepancy implies that con-

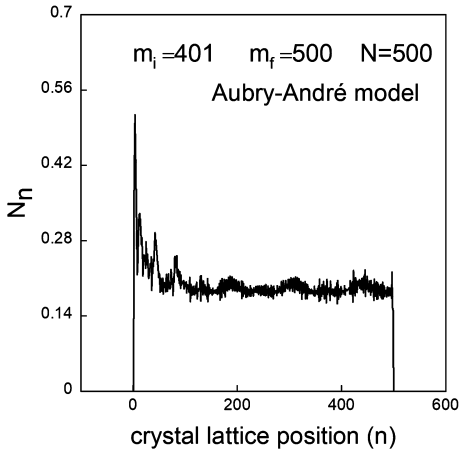

Fig. 8. $\mathcal{N}_n(m_i, m_f)$ versus crystal lattice position (n). The m_i and m_f values have been set to 401 and 500, respectively. In the Aubry-André model: $\pi\alpha = 0.4$, $\lambda = 0.4$, and $\nu = 0.7$.

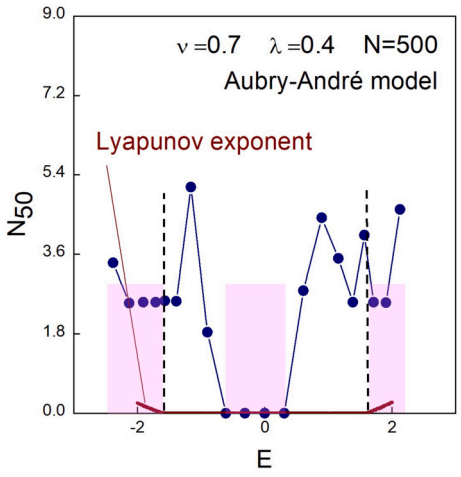

Fig. 9. $\mathcal{N}_{50}$ versus energy for a quasiperiodic potential in an Aubry-André model (dots). It is also shown the Lyapunov exponent versus energy (thick line). In Eq. (3): $\pi\alpha = 0.4$, $\lambda = 0.4$ and $\nu = 0.7$. The dashed lines and the pink stripes indicate the metal-insulator transitions and the energy regions in which the tunneling current is forbidden, respectively. If $\gamma(E) = 0$ or $\mathcal{N}_{50} = 0$, carrier transport through the optical lattice can be neglected.

ductivity through the lattice will be suppressed, as hopping tunneling vanishes in the middle of the energy band. To gain a better understanding of this effect, we calculate a local number of states, denoted as $\mathcal{N}_{50}$, considering the first 50 lattice sites:

$$\mathcal{N}_{50}(m_i, m_f) = \sum_{n=1}^{25} \mathcal{N}_n(m_i, m_f), \tag{9}$$

where $\mathcal{N}_{50}(m_i, m_f)$ is calculated for each 25 consecutive eigenvalues, i.e., $(m_i, m_f) \in \{(1, 25), (26, 50), (51, 75), \ldots\}$.

Fig. 9 shows $\mathcal{N}_{50}$ versus energy for the first 50 lattice sites, along with the plot of the Lyapunov exponent versus energy for an slowly-varying model. We have used $\nu = 0.7$, $\pi\alpha = 0.4$, and $\lambda = 0.4$ for this calculation. The dashed lines in Fig. 9 represent the mobility edges, which are located at $E_c = \pm 1.6$. According to the Lyapunov exponent criteria, the eigenstates localized between these dashed lines are extended states.

However, Fig. 9 clearly demonstrates that $\mathcal{N}_{50}$ vanishes at $|E| \sim 0$, where the eigenstates are extended. We know that the tunneling transport decreases as we decrease $\mathcal{N}_{50}$. As a result, hopping tunneling between the left reservoir and lattice states can be neglected at the

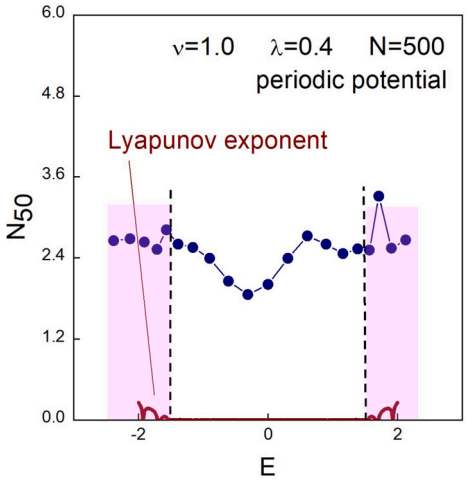

Fig. 10. $\mathcal{N}_{50}$ versus energy for a periodic potential. The Lyapunov exponent versus energy is also shown (thick line). In Eq. (3): $\pi\alpha = 0.4$, $\lambda = 0.4$, and $\nu = 1.0$. The dashed lines and the pink stripes indicate the metal-insulator transitions and the energy regions in which the tunneling current is forbidden, respectively. If $\gamma(E) = 0$ or $\mathcal{N}_{50} = 0$, carrier transport through the optical lattice can be neglected.

band center. Consequently, the conductivity will be suppressed at energies around $E = 0$. This effect must be considered in experiments. Despite having extended states in the middle of the energy band, electron or cold-atom conductivity cannot be expected at energies around $E = 0$ due to the suppression of the tunneling effect. To have a nonzero carrier transport through the optical lattice, we need $\gamma(E) = 0$ and, simultaneously, a finite value for both $\mathcal{N}_{50}$ and $\rho(E)$.

Next, we consider a periodic potential with similar characteristics to the previously employed slowly-varying potential in this work. Specifically, $\nu = 1.0$, $\pi\alpha = 0.4$, and $\lambda = 0.4$ values have been taken in Fig. 10. In Fig. 10, $\pi\alpha = 0.4$ is a real number, the tight-binding chain is not infinite ($N = 500$), and n is an integer. Strictly speaking, the potential is almost periodic.

Fig. 10 presents $\mathcal{N}_{50}$ versus energy in the periodic case, and the Lyapunov exponent is also plotted. It is evident that $\mathcal{N}_{50}$ does not vanish at the band center, indicating that a finite value for the wave function overlap between the reservoir and carrier eigenstates can be expected at energies around $E = 0$. Consequently, electrons and ultracold atoms initially located in the left reservoir can freely tunnel through the crystal potential.

Figs. 9 and 10 demonstrate a fundamental difference between both periodic and quasiperiodic cases. For a slowly-varying potential, the carrier transport through the device vanishes in the middle of the energy band. A similar result, as shown in Figs. 9 and 10, has been obtained for $\nu = 0.6$ and $\nu = 0.8$. Recently, Chakrian et al. [35] studied metallic-insulator phase transitions in an extended Harper model. They used a slowly-varying function with characteristics similar to the potential used in this work and observed a metal-insulator transition as a function of ν. Taking this into account, we believe that it could be interesting to conduct a general study of the tunneling properties as a function of the parameter ν in the near future.

In conclusion, we believe that this effect can be experimentally observed. A solid-state superlattice or an optical lattice can be employed to detect the suppression of tunnel transport in the device (Fig. 9). Fig. 1 illustrates the scheme of the detection mechanism, where electrons or ultracold atoms can be injected into the device through current contacts. To measure the wave function overlap (i.e., the $\mathcal{N}_{50}$ parameter), tunneling experiments through a device with a slowly-varying potential can be considered. The measured tunneling current will be proportional to the wave function overlap, as predicted by Fermi's Golden Rule. Consequently, we can measure the current at different E_F values. When E_F

matches the band center, a suppression of the tunneling current can be expected. Subsequently, electric or atomic currents through the device can be measured using any standard technique.

4. Conclusions

In this study, we have investigated the suppression of hopping transport through a quasiperiodic potential when an aperiodic device is embedded between two electron or ultracold atom reservoirs. Using a one-dimensional tight-binding model, we calculated the local number of states $\mathcal{N}_{50}$ near one of the contacts. Notably, we found that the $\mathcal{N}_{50}$ value near one of the contacts vanishes at energies around $E \sim 0$ in an Aubry-André model. To gain more insights, we compared the quasiperiodic results with those of a periodic potential exhibiting similar characteristics. In the case of a periodic potential, the tunnel conductivity in the device remains unaffected. Our findings suggest that the suppression of the tunneling effect in the middle of the energy band can significantly impact the interpretation of experimental results. This effect can play a fundamental role in understanding the transport properties of the device when a slowly-varying potential is employed. On the other hand, in the case of a periodic potential, electron or ultracold atom conductivity is not suppressed, allowing for freer tunneling through the crystal potential. In conclusion, our study sheds light on the distinctive behavior of hopping transport in quasiperiodic and periodic potentials. Understanding the role of the tunneling effect is crucial for the accurate interpretation and design of experiments involving solid-state superlattices or optical lattices. By further exploring these phenomena, we can unlock new possibilities for developing novel optical and electrical devices based on the peculiar characteristics of quasiperiodic potentials.

CRediT authorship contribution statement

M. Cruz-Méndez: Software, Methodology, Investigation. **H. Cruz:** Writing – review & editing, Writing – original draft, Supervision, Formal analysis, Conceptualization.

Declaration of competing interest

The authors declare that they have no known competing financial interests or personal relationships that could have appeared to influence the work reported in this paper.

Data availability

No data was used for the research described in the article.

References

[1] P.W. Anderson, Phys. Rev. 109 (1958) 1492, https://doi.org/10.1103/PhysRev.109.1492.
[2] S. Aubry, G. André, Ann. Isr. Phys. Soc. 3 (1980) 133.
[3] G.A. Domínguez-Castro, R. Paredes, Eur. J. Phys. 40 (2019) 045403, https://doi.org/10.1088/1361-6404/ab1670.
[4] D. Dutta, A. Roy, K. Saha, Phys. Rev. B 107 (2023) 035120, https://doi.org/10.1103/PhysRevB.107.035120.
[5] J. Billy, V. Josse, Z. Zuo, A. Bernard, B. Hambrecht, P. Lugan, D. Clément, L. Sanchez-Palencia, P. Bouyer, A. Aspect, Nature (London) 453 (2008) 891, https://doi.org/10.1038/nature07000.
[6] S.S. Kondov, W.R. McGehee, J.J. Zirbel, B. DeMarco, Science 334 (2011) 66, https://doi.org/10.1126/science.120901.
[7] K. Huang, D. Vu, X. Li, S. Das Sarma, Phys. Rev. B 107 (2023) 035129, https://doi.org/10.1103/PhysRevB.107.035129.
[8] J. Sutradhar, S. Mukerjee, R. Pandit, S. Banerjee, Phys. Rev. B 99 (2019) 224204, https://doi.org/10.1103/PhysRevB.99.224204.
[9] D. Vu, K. Huang, X. Li, S. Das Sarma, Phys. Rev. Lett. 128 (2022) 146601, https://doi.org/10.1103/PhysRevLett.128.146601.
[10] R.B. Diener, G.A. Georgakis, J. Zhong, M. Raizen, Q. Niu, Phys. Rev. A 64 (2001) 033416, https://doi.org/10.1103/PhysRevA.64.033416.
[11] S. Xu, X. Li, Yi-Ting Hsu, B. Swingle, S. Das Sarma, Phys. Rev. Res. 1 (2019) 032039(R), https://doi.org/10.1103/PhysRevResearch.1.032039.
[12] S. Ray, A. Ghosh, S. Sinha, Phys. Rev. E 97 (2018) 010101(R), https://doi.org/10.1103/PhysRevE.97.010101.
[13] S. Ray, S. Sinha, K. Sengupta, Phys. Rev. A 98 (2018) 053631, https://doi.org/10.1103/PhysRevA.98.053631.
[14] M. Greiner, S. Fölling, Nature 453 (2008) 736, https://doi.org/10.1038/453736a.
[15] Ai-Xia Zhang, Xiao-Wen Hu, Wei Zhang, Jun-Cheng Liang, Ju-Kui Xue, Phys. Lett. A 456 (2022) 128529, https://doi.org/10.1016/j.physleta.2022.128529.
[16] C.B. Tabi, P. Otlaadisa, T.C. Kofané, Phys. Lett. A 481 (2023) 129004, https://doi.org/10.1016/j.physleta.2023.129004.
[17] Jayanta Bera, Barun Halder, Suranjana Ghosh, Ray-Kuang Lee, Utpal Roy, Phys. Lett. A 453 (2022) 128484, https://doi.org/10.1016/j.physleta.2022.128484.
[18] Qing-Li Zhu, Lihua Pan, Phys. Lett. A 481 (2023) 129005, https://doi.org/10.1016/j.physleta.2023.129005.
[19] H. Cruz, Physica E 153 (2023) 115779, https://doi.org/10.1016/j.physe.2023.115779.
[20] R. Masrour, A. Jabar, Solid State Commun. 291 (2019) 15–20, https://doi.org/10.1016/j.ssc.1019.01.004.
[21] E.J. Guzmán, O. Oubram, O. Navarro, I. Rodríguez-Vargas, Phys. Rev. B 107 (2023) 045407, https://doi.org/10.1103/Phys.Rev.B.107.045407.
[22] D.N. Talwar, P. Becla, Physica B 650 (2023) 414500, https://doi.org/10.1016/jphysb.2022.414500.
[23] I.S.F. Bezerra, J.R.F. Lima, Solid State Commun. 340 (2021) 114511, https://doi.org/10.1016/j.ssc.2021.114511.
[24] T. Yoshihiro, N. Nishiguchi, Phys. Rev. B 100 (2019) 235441, https://doi.org/10.1103/PhysRevB.100.235441.
[25] R. Hu, Z. Tian, Phys. Rev. B 103 (2021) 045304, https://doi.org/10.1103/PhysRevB.103.045304.
[26] T. Juntunen, O. Vänskä, I. Tittonen, Phys. Rev. Lett. 122 (2019) 105901, https://doi.org/10.1103/PhysRevLett.122.105901.
[27] S. Das Sarma, S. He, X.C. Xie, Phys. Rev. B 41 (1990) 5544, https://doi.org/10.1103/PhysRevB.41.5544.
[28] A. Esmailpour, M. Esmaeilzadeh, E. Faizabadi, P. Carpena, M. Reza Rahimi Tabar, Phys. Rev. B 74 (2006) 024206, https://doi.org/10.1103/PhysRevB.74.024206.
[29] R.A. Pepino, W.P. Teh, L.J. Magness, New J. Phys. 18 (2016) 013031, https://doi.org/10.1088/1367-2630/18/1/011001.
[30] H. Cruz, S. Das Sarma, J. Phys. I Fr. 3 (1993) 1515, https://doi.org/10.1051/jp1:1993197.
[31] H. Cruz, Acta Phys. Pol. A 133 (2018) 1347, https://doi.org/10.12693/APhysPolA.133.1347.
[32] P. Cruz, H. Cruz, Acta Phys. Pol. A 138 (2020) 21, https://doi.org/10.12693/APhysPolA.138.21.
[33] Xiao Li, Xiaopeng Li, S. Das Sarma, Phys. Rev. B 96 (2017) 085119, https://doi.org/10.1103/PhysRevB.96.085119.
[34] D.J. Boers, B. Goedeke, D. Hinrichs, M. Holthaus, Phys. Rev. A 75 (2007) 063404, https://doi.org/10.1103/PhysRevA.75.063404.
[35] J. Chakrian, M.L. Lyra, J.R.F. Lima, Metallic-insulator phase transitions in the extended Harper model, arXiv:2304.13078.